Electronic properties of Fabre charge-transfer salts under various temperature and pressure conditions

A. C. Jacko,[1] H. Feldner,[1] E. Rose,[2] F. Lissner,[3] M. Dressel,[2] Roser Valentí,[1] and Harald O. Jeschke[1]

[1]*Institut für Theoretische Physik, Goethe-Universität Frankfurt, Max-von-Laue-Straße 1, 60438 Frankfurt am Main, Germany*

[2]*1. Physikalisches Institut, Universität Stuttgart, Pfaffenwaldring 57, 70550 Stuttgart, Germany*

[3]*Institut für Anorganische Chemie, Universität Stuttgart, Pfaffenwaldring 55, 70550 Stuttgart, Germany*

(Received 8 February 2013; published 22 April 2013)

Using density functional theory, we determine parameters of tight-binding Hamiltonians for a variety of Fabre charge transfer salts, focusing, in particular, on the effects of temperature and pressure. Besides relying on previously published crystal structures, we experimentally determine two new sets of structures: $(TMTTF)_2SbF_6$ at different temperatures and $(TMTTF)_2PF_6$ under various hydrostatic pressures. We find that a few trends in the electronic behavior can be connected to the complex phase diagram shown by these materials. Decreasing temperature and increasing pressure cause the systems to become more two dimensional. We analyze the importance of correlations by considering an extended Hubbard model parameterized using Wannier orbital overlaps and show that while charge order is strongly activated by the intersite Coulomb interaction, the magnetic order is only weakly enhanced. Both orders are suppressed when the effective pressure is increased.

DOI: 10.1103/PhysRevB.87.155139 PACS number(s): 71.15.Mb, 71.10.Fd, 71.20.−b, 61.66.Hq

I. INTRODUCTION

Quasi-one-dimensional organic salts formed from tetramethyltetrathiafulvalene (TMTTF) molecules—also known as Fabre charge-transfer (CT) salts—have been intensively investigated in the last two decades since they exhibit a rich variety of phases like antiferromagnetism, superconductivity, charge ordering, spin-density wave ordering, or spin-Peierls behavior.[1–3] Such phases can be driven both by external (physical) pressure as well as by chemical pressure (see Fig. 1). Even though a few successful models have been proposed for the description of these systems, constructing a consistent microscopic picture of the relationships between the various phases remains a challenge.[5–7]

The primary avenue of the present work is to understand the microscopic origin of the close competition between the different phases in these compounds as a function of chemical and external pressure as well as temperature. For that, we performed *ab initio* density functional theory (DFT)[8,9] and model Hamiltonian calculations for several Fabre CT salts whose crystal structures were determined at different temperatures and pressures and investigated variations of their electronic properties with temperature and pressure.[10] By computing the real-space overlaps of Wannier orbitals for the bands near the Fermi level, we parameterize a two-band tight-binding Hamiltonian model for the various systems and examine the differences in their electronic hopping parameters. In this way, we can connect structural and chemical modifications with changes in the electronic properties. Furthermore, in order to analyze some of the preferred orderings, we consider a description of the Fabre CT salts in terms of an extended Hubbard Hamiltonian including on-site and intersite Coulomb interaction terms. The kinetic part of this model is given by the computed hopping parameters for the various compounds. We discuss spin-spin and charge-charge correlation properties by diagonalizing the model.

The work is organized as follows. Sections II and III are dedicated to the description of the computational details as well as the crystal structure of the Fabre CT salts. In Secs. IV–VI, we present, respectively, our results on the electronic structure, tight-binding models as well as extended Hubbard models for a few members of Fabre CT salts. Discussion and conclusions are given in Secs. VII and VIII.

II. COMPUTATIONAL DETAILS

The electronic structure calculations presented here were performed in an all-electron full-potential local orbital basis using the FPLO package.[15] The densities were converged on an $(8 \times 8 \times 8)$ k mesh, using a generalized gradient approximation (GGA) functional.[16]

For materials without published hydrogen coordinates, hydrogen atoms were placed according to the expected bond lengths and angles of a methyl group (C-H distance 1.1 Å, C-C-H angle 109°). With the bond length and angle fixed, one has the freedom to choose the rotation angle of the set of hydrogen atoms on each methyl group around the C-C bond. We chose this angle such that one hydrogen is as far out of the plane of the molecule as possible. We tested the effect of this choice on the band structure and found no contribution to the bands of interest near the Fermi level since in this energy region only TMTTF bands of π origin are involved.

Some of the structures had unexpected bond lengths and angles; therefore the atomic coordinates were relaxed with DFT using the Vienna *ab initio* simulation package (VASP, version 5.2.11),[17,18] with a projector-augmented wave basis.[19,20] We used the GGA functional,[16] and included van der Waals corrections[21] for the relaxations. The atomic coordinates were converged to an energy difference of 1 meV on a $(5 \times 5 \times 5)$ k mesh, with a plane wave cutoff energy of 500 eV. We performed two kinds of relaxations; in one relaxation, we kept sulfur and the heavy anion atomic coordinates fixed, and in the other relaxation, all atom positions were relaxed. The differences between the two relaxed structures were minimal. Overall, apart from the suspicious sites, the relaxed structures were slightly bent with respect to the experimental structure

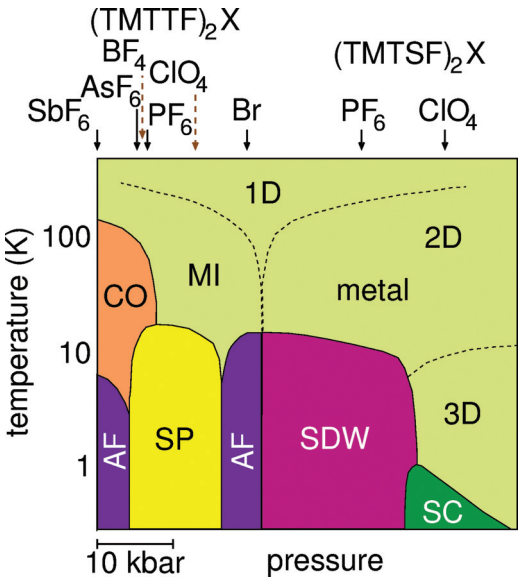

FIG. 1. (Color online) Temperature-pressure phase diagram for the TMTTF and TMTSF charge transfer salts, as first suggested in Ref. 1 and refined by many others. Position in the phase diagram can be tuned by physical (in this case hydrostatic), or chemical (changing anion) pressure. The ambient pressure position for each salt is indicated with an arrow above the diagram. An increase of pressure (external or chemical) causes the system to be less one dimensional. The possible phases are charge ordered (CO), Mott insulating (MI), antiferromagnetic (AF), spin Peierls (SP), spin density wave (SDW), superconducting (SC), and 1D, 2D, or 3D metal. The positions of $(TMTTF)_2ClO_4$ and $(TMTTF)_2BF_4$ are not well known. In the phase diagram, their approximate positions have been indicated with dashed arrows. These two anions break the inversion symmetry of the system, allowing for an anion ordering transition. After they go through this transition (between 40 and 75 K), the shown phase diagram is no longer relevant.[4] More work is needed to understand the physics of these two systems at low temperatures, but it seems that just considering effective pressure will not be sufficient.

(by fractions of an angstrom), with the central atoms moving slightly further from the other monomer in the unit cell, the sulfurs remaining nearly fixed, and the methyl groups bending slightly towards those of the other monomer. These changes maintain the inversion symmetry relating the two TMTTF molecules in each unit cell, and slightly shifts the center of mass, reducing the structural dimerization of the chains slightly relative to the unrelaxed structures.

The tight-binding parameters were obtained by constructing Wannier orbitals for the TMTTF bands at the Fermi level and computing real-space overlaps, as implemented in FPLO. Another way to generate these parameters is to fit the band structure of the model Hamiltonian to the DFT bands. The latter method can become difficult when many hopping parameters need to be fitted; there can be a number of solutions that reproduce the DFT bands equally well, but differ in physical details (such as relative strengths of certain bonds). By using Wannier orbital overlaps, we can be sure that our parameter values have a clear physical interpretation. The exact diagonalization of the extended Hubbard model was performed by considering system sizes of 4×4 TMTTF sites with periodic boundary conditions.

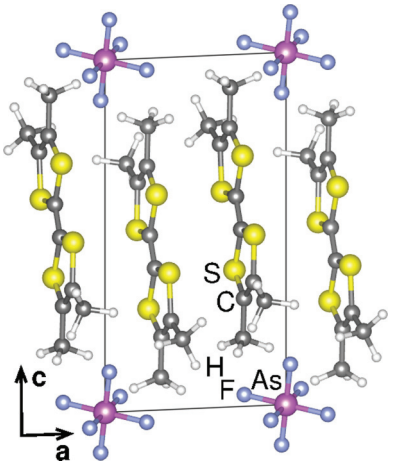

FIG. 2. (Color online) Crystal structure of the Fabre CT salts projected into the ac plane. The organic molecules form π-stacked 1D chains along the crystal a direction (with a slight zigzag pattern) and form layers parallel to the ab plane. These organic layers alternate with anion layers (with the anions centered on the pink As sites) stacked in the c direction. Grey atoms are carbon, yellow are sulfur, while hydrogen atoms are shown in white.

III. CRYSTAL STRUCTURE

The Fabre CT salts consist of alternate layers of TMTTF molecules (cations) and monovalent anions, stacked in the c direction (see Fig. 2). In between the cation layers, the planar TMTTF molecules form π-stacked one dimensional chains in the a direction with a slight "zigzag" arrangement. There is a charge transfer of one electron from each $(TMTTF)_2$ dimer to each anion, i.e., the TMTTF molecules carry half a hole on average. There are two classes of anions: those that conform to the $P\bar{1}$ symmetry of the TMTTF part of the crystal (such as PF_6), and those that break that symmetry (such as ClO_4). Also, the anion species influence the proportions of the unit cell as well as the intra- and inter-chain hopping strengths. The interchain hopping strengths are not only determined by the distance between the TMTTF molecules, but also by changes in their zigzag arrangement (that is to say, how far away from a perfectly aligned stack they are and in what direction).

TMTTF molecules within a chain show a slight dimerization along the chain. We can quantify this structural dimerization as the difference between the larger dimerization distance of adjacent TMTTF molecules, d_1, and the shorter dimerization distance d_0, normalized by the sum of the two distances:

$$\partial_{\text{struc}} = 2\frac{d_1 - d_0}{d_1 + d_0}. \quad (1)$$

These distances are defined as the distances between the centres of mass of the C and S atoms in each TMTTF molecule.

Table I shows the structural dimerization of the materials investigated in this work. This table also includes the electronic dimerization, which is introduced in Sec. V. In general, the structural dimerization increases slightly with increasing temperature.

Cooling from room temperature to $T = 4$ K, $(TMTTF)_2AsF_6$ and $(TMTTF)_2PF_6$ both show charge ordering phase transitions and spin-Peierls transitions.

TABLE I. Structural and electronic dimerization of the Fabre CT salts considered in the present work. The structural dimerization of the TMTTF molecules is defined in Eq. (1) and the electronic dimerization is defined in Eq. (4) in Sec. V. References marked with * have no (or unrealistic) published hydrogen coordinates. Note that ClO_4 and BF_4 are tetrahedral anions, and so do not conform to the reported $P\bar{1}$ symmetry (the anions do not have the required inversion symmetry). The anion ordering transition only occurs in these systems where the anion does not have inversion symmetry. The change in sign of ∂_{elec} indicates that the shorter bond has the smaller t.

Anion	∂_{struc}	∂_{elec}	Ref.
SbF_6 (100 K)	0.007	0.042	new
SbF_6 (140 K, sample 1)	0.011	0.067	new
SbF_6 (140 K, sample 2)	0.013	0.094	new
SbF_6 (180 K)	0.020	0.115	new
SbF_6 (200 K)	0.023	0.141	new
SbF_6 (300 K, sample 1)	0.047	0.279	new
SbF_6 (300 K, sample 2)	0.041	0.298	new
AsF_6 (4 K)	0.007	0.100	22
PF_6 (4 K)	0.009	0.126	22
AsF_6 (300 K)	0.041	0.110	23*
PF_6 (300 K)	0.040	0.230	new
PF_6 (300 K, 0.3 GPa)	0.018	0.577	12 and 13
PF_6 (300 K, 0.6 GPa)	0.016	0.595	12 and 13
PF_6 (300 K, 0.9 GPa)	0.002	0.477	12 and 13
PF_6 (300 K, 1.5 GPa)	0.003	−0.454	12 and 13
PF_6 (300 K, 2.0 GPa)	0.010	−0.397	12 and 13
PF_6 (300 K, 2.7 GPa)	0.024	−0.183	12 and 13
Br (300 K)	0.019	−0.189	24*
ClO_4 (300 K)	0.040	0.616	25*
BF_4 (100 K)	0.020	−0.054	26
BF_4 (300 K)	0.028	0.336	26

These ordering transitions are not visible in the crystal structures—there are no significant changes in the structural dimerization from $T = 300$ to 4 K. $(TMTTF)_2SbF_6$ also has no significant changes in the structural dimerization between 100 K and room temperature, and goes through a CO transition in this range.

IV. ELECTRONIC STRUCTURE

In the following, we examine the electronic properties of $(TMTTF)_2PF_6$ in detail and will use this analysis as a baseline for understanding the Fabre CT salts. In Fig. 3(a), we present the band structure and density of states of $(TMTTF)_2PF_6$ in a window of energy $[-4\,eV, 4\,eV]$ around the Fermi level. The bands have been drawn along the high-symmetry path shown in the Brillouin zone in Fig. 3(b). It is clear from the partial density of states that near the Fermi level all the bands are predominantly due to the TMTTF molecules. In fact, the nearest anion bands are about 4.1 eV below the Fermi level and more than 10 eV above it. The two 3/4-filled organic bands near the Fermi energy are a common feature of the Fabre salts as a result of hole-doped pairs of TMTTF molecules. In $(TMTTF)_2PF_6$, these bands are well separated from the rest of the bands, with gaps of more than 1 eV to the lower valence bands and upper conduction bands, respectively. The size of the gaps vary with anion type, and sometimes anion bands cross the two TMTTF bands [as in the case of $(TMTTF)_2Br$].

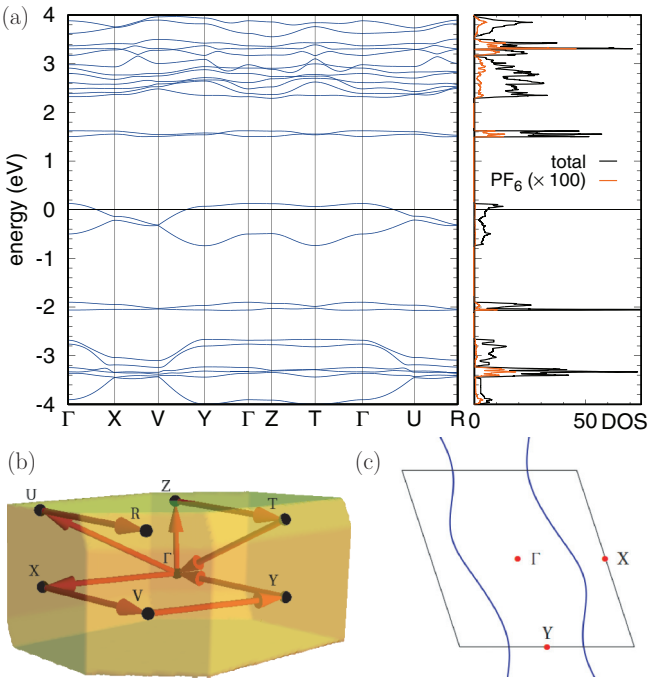

FIG. 3. (Color online) Electronic properties of $(TMTTF)_2PF_6$ ($T = 4$ K structure). (a) Band structure and density of states. (b) Path through k space considered for the band structure plotting. (c) Fermi surface in the $k_z = 0$ plane. The total density of states is shown in black and the partial density of states of the anions (increased by a factor of 100) is shown in orange (dashed). The partial density of states shows that within this energy window, all of the bands in this energy window have predominantly TMTTF character, and the two bands at the Fermi level are nearly purely TMTTF. We find that these general features of the bands and density of states are consistent across the TMTTF salts studied here with the exception of $(TMTTF)_2Br$, which has three additional bands (of anion origin) near its Fermi level; the variations in the bands at the Fermi level are discussed further in Sec. V.

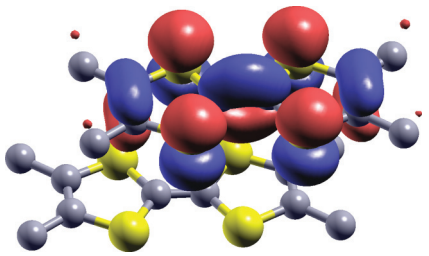

FIG. 4. (Color online) The two TMTTF molecules of a unit cell, along with one of the Wannier orbitals of $(TMTTF)_2PF_6$ for the bands near the Fermi level. It is clear that this Wannier orbital has the structure of the HOMO of a TMTTF molecule in the gas phase. The other Wannier orbital needed to describe the two organic bands corresponds to the HOMO of the other TMTTF molecule in the unit cell (and is related to the first one by inversion symmetry). This is in agreement with the information in the partial density of states [see Fig. 3(a)]; the orbitals near the Fermi energy are predominantly of TMTTF nature.

The quasi-one-dimensionality of this system is manifested in the band structure [see Fig. 3(a)] where we find very little dispersion in the k_y and k_z directions and bands only cross the Fermi level in the k_x direction. This can be also observed in the Fermi surface cut at $k_z = 0$ shown in Fig. 3(c). This quasi-one-dimensional behavior is a typical feature of the Fabre CT salts.

In order to further characterize the electronic structure of these systems, we generate Wannier orbitals for the two organic bands near the Fermi level as described in Sec. I. An example is shown in Fig. 4. These bands have the symmetry of the TMTTF highest occupied molecular orbitals (HOMOs), partially depopulated by the charge transfer of one electron from a pair of TMTTF molecules to the anion layer. These two bands determine the low-energy physics of these systems and, in what follows, we shall concentrate on the analysis of this band manifold. We note that we are not considering DFT calculations beyond GGA and therefore leave correlation effects (beyond GGA) to be explicitly treated in the model calculations.

V. TIGHT-BINDING MODEL

Wannier orbitals form a natural basis for a tight-binding model. By computing overlaps between the orbitals, we can parametrize the two HOMO bands at the Fermi energy in terms of a two-site tight-binding Hamiltonian where the lattice sites are defined as the centers of mass of the two TMTTF molecules in each unit cell:

$$\hat{H}_N = \mu \sum_i c_i^\dagger c_i - \sum_{\langle i,j\rangle_N} t_{ij} c_i^\dagger c_j, \tag{2}$$

μ is the on-site energy, t_{ij} are hopping parameters between sites i and j, and the sum over $\langle i,j\rangle_N$ indicates that only hoppings up to the Nth nearest neighbor are included. This is a model of the lattice of TMTTF monomers. In listing hopping parameters, we will use

$$t_{ij} \equiv t_\alpha(r_{ij}), \tag{3}$$

where r_{ij} are distances between TMTTF centers of mass and $\alpha = 0,1,2,\ldots$ counts neighbor distances in ascending order. In the discussion that follows, we include hoppings up to the eighth nearest neighbor ($N = 8$). These eight hopping terms do not include any inter-layer hopping, and therefore the resulting tight-binding bands have no dispersion in the k_z direction. The resulting tight-binding parameters for the eight shortest inter-site distances are shown in Table II. The longer hopping terms are of the same order as t_7 or smaller.

A. Anion dependence of the structural and electronic properties

In Fig. 5, we show the band structure of the various Fabre CT salts considered in this study with crystal structures measured

TABLE II. t_α Values determined from the Wannier orbitals for all TMTTF structures investigated here (energies in eV). The t_α are numbered from shortest to longest bond (defined by distance between the centres of mass of the TMTTF molecules), except where noted below.[47] It is clear that the intrachain terms, t_0 and t_1, are the dominant hopping terms. Note that for $(TMTTF)_2PF_6$ above 0.9 GPa, for Br at room temperature and for BF_4 at 100 K, the dominant in-chain t is the longer one; we have swapped the labels for these materials such that t_0 remains the strongest in-chain coupling. The labels (A) and (B) refer to the two inequivalent TMTTF molecules in each unit cell (in the absence of inversion symmetry).

Anion	μ	t_0	t_1	t_2	t_3	t_4	t_5	t_6	t_7	optimized
SbF_6 100 K	−0.2516	0.1823	0.1747	−0.0344	−0.0030	0.0310	−0.0104	0.0018	−0.0027	yes
SbF_6 140 K (1)	−0.2459	0.1810	0.1692	−0.0285	−0.0029	0.0314	−0.0061	0.0009	−0.0027	yes
SbF_6 140 K (2)	−0.2486	0.1853	0.1687	−0.0279	−0.0029	0.0318	−0.0059	0.0008	−0.0030	yes
SbF_6 180 K	−0.2449	0.1853	0.1652	−0.0193	−0.0029	0.0283	0.0010	0.0001	−0.0020	yes
SbF_6 200 K	−0.2417	0.1857	0.1612	−0.0138	−0.0029	0.0259	0.0053	−0.0004	−0.0013	yes
SbF_6 300 K (1)	−0.2379	0.1947	0.1470	0.0023	−0.0032	0.0176	0.0146	−0.0000	−0.0010	yes
SbF_6 300 K (2)	−0.2342	0.1925	0.1426	0.0043	−0.0034	0.0140	0.0129	0.0012	−0.0007	yes
AsF_6 4 K	−0.2617	0.1943	0.1759	−0.0380	−0.0038	0.0358	−0.0141	0.0015	−0.0051	no
PF_6 4 K	−0.2539	0.1912	0.1686	−0.0333	−0.0038	0.0367	−0.0104	0.0008	−0.0052	no
AsF_6 300 K	−0.2292	0.1751	0.1568	−0.0076	−0.0047	0.0188	0.0244	0.0010	−0.0021	yes
PF_6 300 K	−0.2477	0.1976	0.1569	−0.0025	−0.0141	0.0030	0.0312	−0.0003	−0.0035	yes
PF_6 300 K, 0.3 GPa	−0.2203	0.1981	0.1093	0.0059	−0.0056	0.0278	−0.0094	0.0015	−0.0063	yes
PF_6 300 K, 0.6 GPa	−0.2280	0.2065	0.1118	0.0108	−0.0062	0.0291	−0.0090	0.0009	−0.0066	yes
PF_6 300 K, 0.9 GPa	−0.2513	0.2193	0.1348	0.0019	−0.0065	0.0349	−0.0085	0.0003	−0.0085	yes
PF_6 300 K, 1.5 GPa	−0.2550	0.2207	0.1390	0.0015	−0.0080	0.0378	−0.0136	0.0001	−0.0086	yes
PF_6 300 K, 2.0 GPa	−0.2757	0.2333	0.1561	−0.0041	−0.0092	0.0408	−0.0159	−0.0000	−0.0093	yes
PF_6 300 K, 2.7 GPa	−0.3081	0.2398	0.1996	−0.0199	−0.0092	0.0513	−0.0154	−0.0015	−0.0099	yes
Br 300 K	−0.2215	0.1719	0.1422	−0.0270	−0.0048	0.0311	0.0025	−0.0007	−0.0005	yes
ClO_4 300 K (A)	−0.2195	0.2017	0.1067	−0.0022	−0.0042	0.0313	−0.0136	0.0010	−0.0081	no
ClO_4 300 K (B)	−0.2289	0.2017	0.1067	−0.0022	−0.0050	0.0320	−0.0136	0.0011	−0.0081	no
BF_4 100 K (A)	−0.2435	0.1735	0.1644	−0.0151	−0.0063	0.0296	−0.0240	0.0004	0.0210	no
BF_4 100 K (B)	−0.2353	0.1735	0.1644	−0.0151	−0.0062	0.0300	−0.0240	0.0015	0.0210	no
BF_4 300 K (A)	−0.2618	0.2057	0.1466	−0.0209	−0.0010	0.0381	−0.0220	−0.0013	−0.0032	no
BF_4 300 K (B)	−0.2413	0.2057	0.1466	−0.0209	−0.0007	0.0373	−0.0220	−0.0013	−0.0032	no

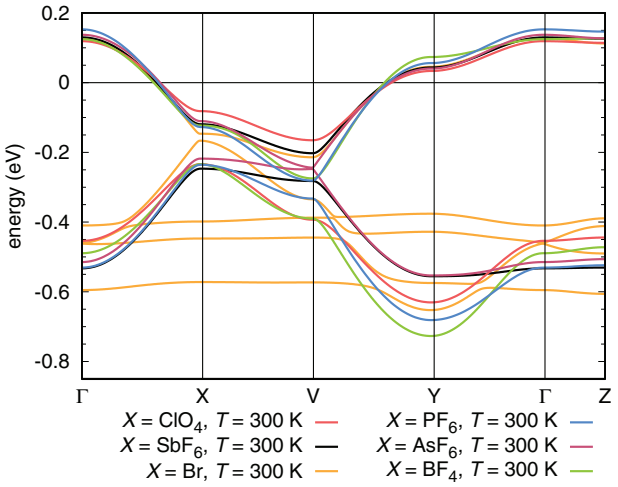

FIG. 5. (Color online) Band structures in the energy window [−0.8 eV,0.2 eV] of the TMTTF salts with crystal structures measured at ambient pressure and room temperature. In this energy range, all of the materials shown here have two bands arising from TMTTF HOMO orbitals. The $(TMTTF)_2Br$ salt additionally has three anion bands within this window. The common TMTTF bands differ in details; between Γ and X (corresponding to the in-chain direction) the bands are very similar. There is more variation in the inter-chain direction, indicating the differing degrees of interchain coupling.

at ambient pressure and room temperature (see Table I). This comparison allows us to analyze the effects of chemical pressure (i.e., anion substitution) on the electronic properties. For $(TMTTF)_2Br$ there are three additional Br bands crossing the lower organic band.

We observe that the TMTTF bands vary only modestly with anion at a given temperature, particularly at the Γ and Z points. The largest difference in the band structure is seen along the X-V path, [$X = (0.5,0,0)$, $V = (0.5,0.5,0)$ in units of the reciprocal lattice vectors] where the indirect influence of the anion is most prominent. It is clear that in $(TMTTF)_2Br$ strong mixing with the Br bands distorts the TMTTF bands around the avoided crossings. Away from the avoided crossings the bands are similar to the TMTTF bands observed for the other salts. It is worth noting that $(TMTTF)_2Br$ is the only salt studied here with easily accessible metallic and superconducting states.[27]

In Fig. 6, we show the real-space network of hopping terms t_{ij} [see Eq. (3)] between TMTTF molecules computed from the Wannier orbitals overlaps for $(TMTTF)_2AsF_6$ [see Fig. 6(a)] and $(TMTTF)_2ClO_4$ [see Fig. 6(b)]. The strength of the hopping is linearly encoded into the bond diameter. This figure shows that these materials have a preferred hopping direction (the direction with the thickest bonds), forming one-dimensional chains. The ratio of inter to intrachain hopping strengths is smaller in $(TMTTF)_2AsF_6$ than in $(TMTTF)_2ClO_4$, which indicates that $(TMTTF)_2AsF_6$ is more one dimensional.

While all of the materials have strong intrachain hopping terms [of order ∼0.15–0.25 eV)], the interchain hopping terms can vary by about an order of magnitude (see Table II). The values of the intrachain hopping parameters in our work are consistent with those found for similar systems in previous experimental and theoretical investigations.[27–33] Missing in

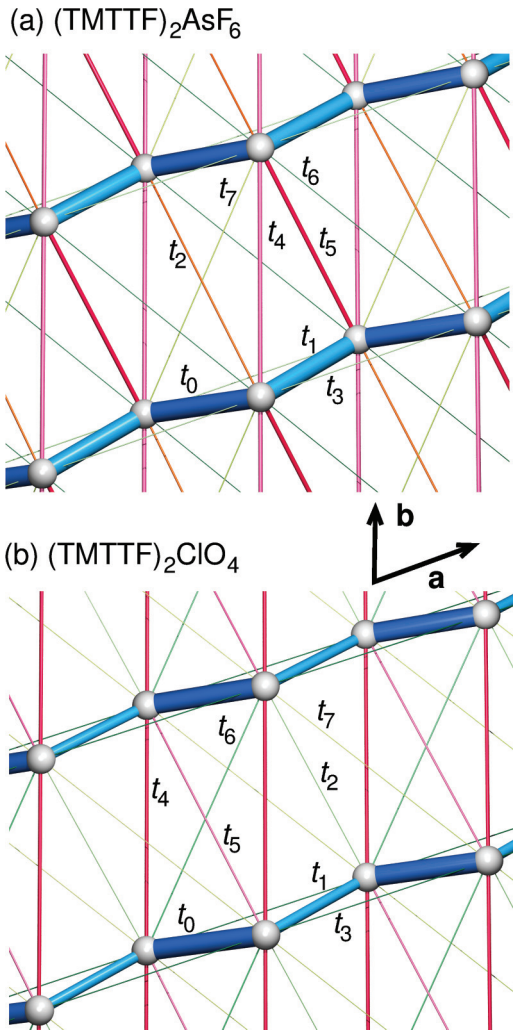

FIG. 6. (Color online) Visualization of the strength of the hopping between the sites of the tight-binding model, the centers of mass of the TMTTF molecules (gray spheres); shown for (a) $(TMTTF)_2AsF_6$ and (b) $(TMTTF)_2ClO_4$ (both at room temperature). The diameter of the bonds is proportional to the tight-binding parameter strength $|t_\alpha|$. $|t_\alpha|$ above 0.1 eV are each a different shade of blue, $|t_\alpha|$ between 0.1 eV and 0.01 eV are a shade of red/orange, while $|t_\alpha|$ less than 0.01 eV are a shade of green. See Table II for t_α values.

those previous studies is a thorough analysis of the intrachain dimerization as well as the interchain hopping parameters.

In Table I, we quantify the electronic dimerization for the Fabre CT salts studied in this work analogously as we did for the structural dimerization, i.e.,

$$\partial_{\text{elec}} = 2\frac{t_0 - t_1}{t_0 + t_1}, \tag{4}$$

where t_0 (t_1) is the hopping term corresponding to the smallest (second smallest) bond length. While we observe a significant dependence on the nature of the anion, the structural and electronic dimerizations seem to be uncorrelated. This can be understood physically: the electronic dimerization is defined by hopping integrals whose magnitude depends on the orientation of the overlapping orbitals as well as on their separation. If the orientation is more favorable along the longer

intrachain bond, then the more distant overlap can be larger. This is the case for the structures of $(TMTTF)_2PF_6$ above $P = 0.9$ GPa, $(TMTTF)_2BF_4$ at $T = 100$ K, and $(TMTTF)_2Br$ at room temperature; a negative value of ∂_{elec} in Table I indicates that the longer bond has a larger hopping strength. Focusing on the anions with octahedral symmetry at room temperature, we observe that while the structural dimerization has a consistent trend downwards as the anion changes from $(SbF_6)^-$ through $(AsF_6)^-$ to $(PF_6)^-$ (chemical pressure, smaller volume) and then further downwards as pressure is applied, the electronic dimerization follows the opposite trend with pressure. We will discuss this behavior below.

B. Temperature dependence of the structural and electronic properties

We proceed now with the analysis of the temperature dependence of the structural and electronic behavior of a few Fabre CT salts. This study is done by performing ground-state DFT calculations for structures determined at different temperatures. The investigation for $(TMTTF)_2AsF_6$ and $(TMTTF)_2PF_6$ is done by considering crystal structures obtained experimentally at $T = 4$ and 300 K. The investigation for $(TMTTF)_2SbF_6$ is done using crystal structures determined experimentally at temperatures between $T = 100$ and 300 K.

In Fig. 7, we present the band structure of $(TMTTF)_2SbF_6$ as a function of temperature. Note that we have two sets of structural coordinates at 300 and 140 K, so we have presented the bands and parameters for both. We observe that as the temperature is decreased, the bandwidth increases and the dispersion between X and V becomes steeper; this indicates that the electronic structure becomes more two-dimensional with decreasing temperature. This trend can be also observed in the behavior of the 2D tight-binding parameters (see Fig. 8), especially t_2, t_4, and t_5.

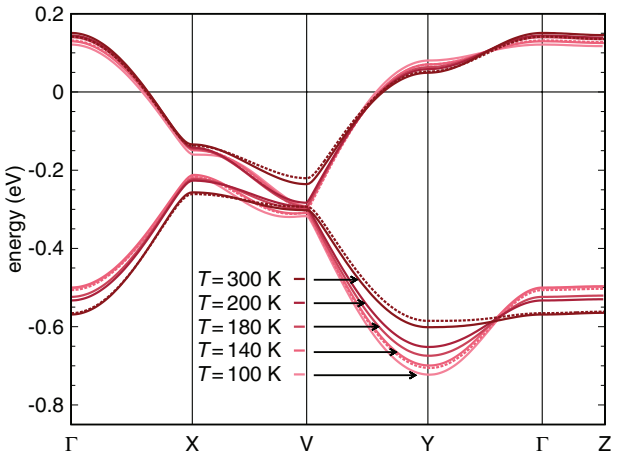

FIG. 7. (Color online) Band structure of $(TMTTF)_2SbF_6$ calculated from the crystal structures obtained at several temperatures between $T = 100$ and 300 K. At $T = 140$ and 300 K, structures from two different samples were used; the additional bands at those temperatures are plotted with dashed lines. As the temperature is decreased, the bandwidth increases and the dispersion between the X and V points becomes steeper; this indicates that the electronic structure becomes more two dimensional with decreasing temperature.

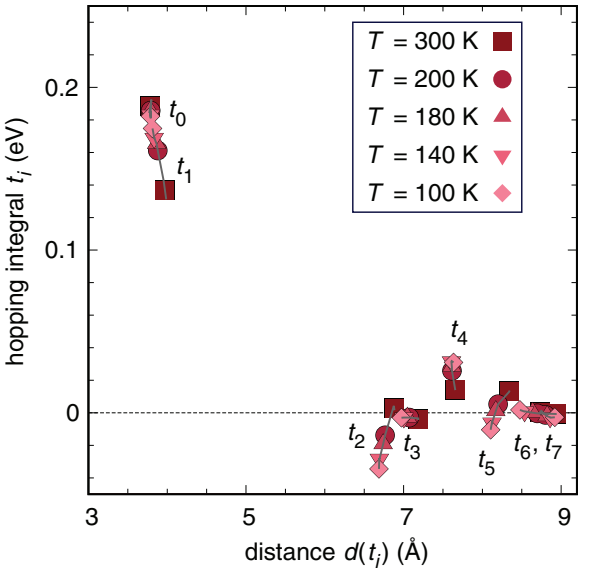

FIG. 8. (Color online) Evolution of tight-binding parameters of $(TMTTF)_2SbF_6$ with temperature. As temperature is lowered to $T = 100$ K, the dominant hoppings t_0 and t_1 become nearly equal, making the TMTTF chain nearly isotropic. The sizable 2D couplings t_2, t_4, and t_5 show a complicated temperature dependence, with t_2 and t_5 changing sign and t_4 increasing considerably as temperature is lowered.

In order to quantify the electronic dimensionality, we introduce a dimensionality parameter D by taking the ratio of the inter-chain hopping terms ($t_\alpha^\perp$) and intrachain hopping terms ($t_\beta^\parallel$),

$$D = \frac{\sum_\alpha |t_\alpha^\perp|}{\sum_\beta |t_\beta^\parallel|}. \quad (5)$$

We emphasize that this parameter is an estimate of a model dimensionality. The correlation between temperature, dimensionality, and bandwidth is seen more clearly by using this parameter, as illustrated in Fig. 9(a), where D for $(TMTTF)_2SbF_6$ increases with decreasing temperature.

In Fig. 10, we present the band structure for $(TMTTF)_2AsF_6$ and $(TMTTF)_2PF_6$ for the crystal structures at $T = 4$ and 300 K. The interchain (X-V path) dispersion increases with decreasing temperature. $(TMTTF)_2AsF_6$ and $(TMTTF)_2PF_6$ undergo spin-Peierls transitions (at $T = 11.4$ and 16.4 K, respectively),[34] however, there is no energy splitting at $T = 4$ K since the crystal structure is not tetramerized. Interestingly, the electronic and structural dimerizations in these systems (see Table I) are larger for the room-temperature structures than for the structures measured at $T = 4$ K.

We also investigated $(TMTTF)_2BF_4$. For this system, the electronic dimerization changes sign since the electronic dimers are on the more closely spaced TMTTF molecules (in terms of center of mass separation) in the room-temperature structure and on the more distant pair for the structure at 100 K.

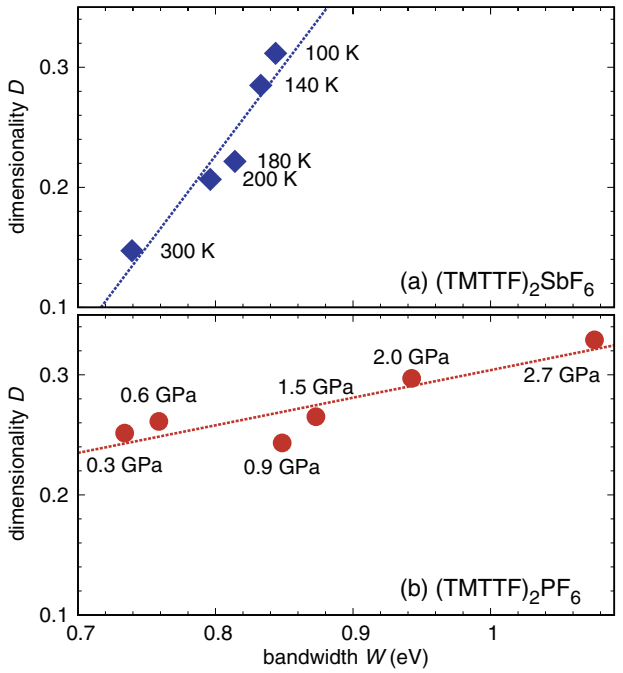

FIG. 9. (Color online) Dimensionality vs bandwidth of $(TMTTF)_2SbF_6$ with temperature (diamonds) and $(TMTTF)_2PF_6$ under pressure (circles); the bandwidth is the energy difference between the highest and lowest energies in the TMTTF bands around the Fermi energy, and the dimensionality is defined by the ratio of the hopping integrals in the intra and interchain directions [see Eq. (5)]. We see the expected positive correlation between bandwidth and pressure (indicated by the arrow): as the pressure increases, so does the intermolecular hopping and therefore the bandwidth. We also see a strong positive correlation between pressure and dimensionality. There is a negative correlation between temperature and dimensionality and bandwidth; increasing the temperature has a similar effect to decreasing the pressure. The 140- and 300-K points for $(TMTTF)_2SbF_6$ are averaged over the two structures available at those temperatures.

C. Pressure dependence of structural and electronic properties

Here, we investigate a series of new experimental crystal structures of $(TMTTF)_2PF_6$ determined at room temperature under various hydrostatic pressures. Figure 11 shows how the band structure evolves as a function of pressure. As the pressure is increased, the bandwidth increases, and the system becomes more two dimensional (i.e., the dispersion is enhanced along the path X-V). This is also apparent in the tight-binding parameters (see Fig. 12); all the parameters grow with pressure (increasing the bandwidth), but not all by the same proportion, changing the degree of two dimensionality. This trend to higher dimensionality has also been observed experimentally. Optical experiments on $(TMTTF)_2PF_6$ under pressure show that the metallic conductivity (Drude spectral weight) changes very anisotropically; it increases quickly with pressure in the perpendicular direction, while in the in-chain direction there is very little change.[13] This trend with pressure has also been seen in other similar systems [$(TMTTF)_2AsF_6$ and $(TMTTF)_2PF_6$] and identified as a crossover from a quasi-1D system to a 2D metal.[35,36]

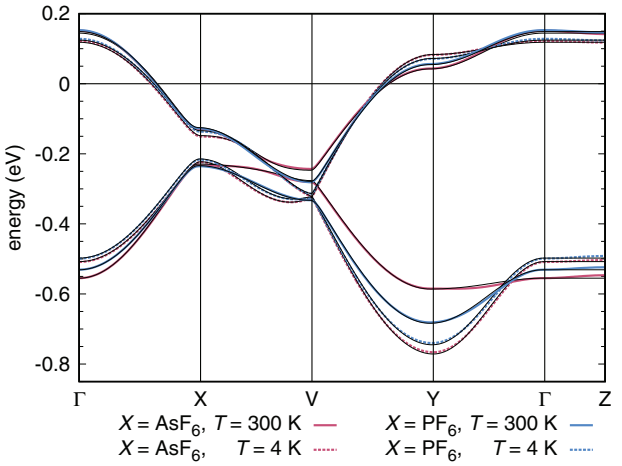

FIG. 10. (Color online) Band structures of $(TMTTF)_2AsF_6$ (red) at $T = 4$ K (dashed) and room temperature (solid line), $(TMTTF)_2PF_6$ (blue) at $T = 4$ K (dashed) and room temperature (solid line). The black lines are the bands resulting from the model Hamiltonian (2), parametrized by the Wannier orbital overlaps for the eight shortest hops. In the model used there is no dispersion in the k_z direction since the eight shortest hops are all in the same plane, i.e., we have a two-dimensional model. It is clear from the DFT bands that the interplanar coupling is small, which is why the 2D model fits so well. Note that $T = 4$ K is below both the charge ordering and spin Peierls transitions of $(TMTTF)_2AsF_6$ and $(TMTTF)_2PF_6$.

Table I shows that between $P = 0.9$ and 1.5 GPa, the TMTTF molecules become almost equally spaced (in terms of the centers of mass) since $\delta_{\text{struct}} \sim 0$. At $P = 1.5$ GPa, the larger interchain hopping is no longer associated to t_0, but to t_1; to avoid a discontinuity, we make an exception to the numbering of t_α with ascending distance and refer, for pressures 1.5 to 2.7 GPa, to the largest hopping as t_0 even though it belongs to the second nearest neighbor distance. The interchain hoppings t_0 and t_1 do not become equal around 1.2 GPa because even when the centers of mass are equally

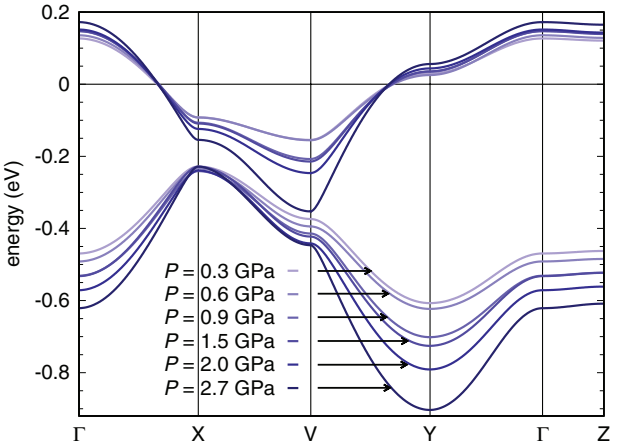

FIG. 11. (Color online) Band structure of $(TMTTF)_2PF_6$ at various pressures. As the pressure is increased, the bandwidth increases, and the dispersion becomes steeper between the X and V points; the system becomes more two dimensional. These trends are made obvious in Fig. 9 (b).

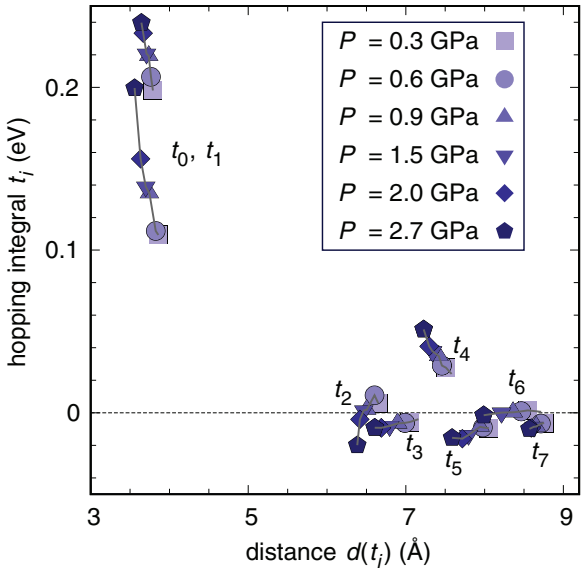

FIG. 12. (Color online) Tight-binding parameters of $(TMTTF)_2PF_6$ at various pressures as a function of distance. Note that as the pressure is increased, the trend is for the t's to become larger. In Fig. 9(b), we see that the increases are such that the system becomes more two dimensional.

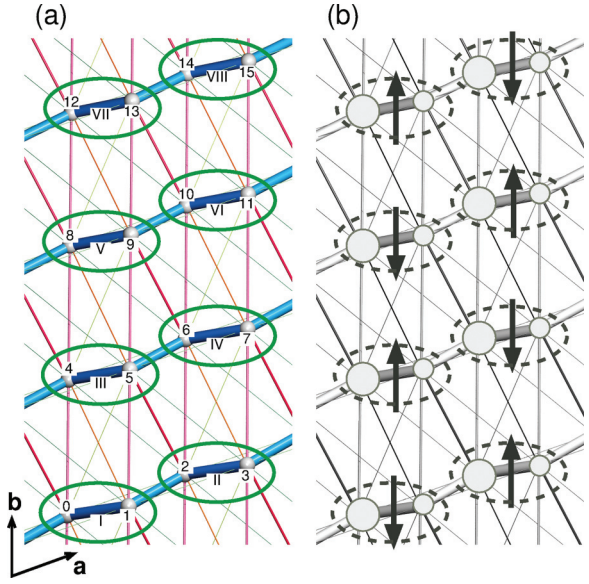

FIG. 13. (Color online) Schematic representation of the TMTTF molecules in the conducting plane for the Fabre salts studied here. (a) Balls correspond to the TMTTF molecules and ellipses indicate the dimers. The site and dimer labeling is shown. (b) A sketch of a possible charge- and magnetically ordered state; the size of the circles represent the hole density, and the arrows the net magnetism.

spaced, the staggering of the molecules in the chain means that the two hopping integrals are not equivalent. At pressures above $P = 1.3$ GPa, $(TMTTF)_2PF_6$ is known experimentally to become metallic, and at low temperatures undergoes a spin-density wave transition.[32,37]

Figure 9(b) shows how the dimensionality and bandwidth of $(TMTTF)_2PF_6$ varies with pressure. We observe the expected trend of increasing bandwidth under pressure (forcing the TMTTF molecules closer together, increasing their intermolecular interactions). We also see that physical pressure changes the bandwidth more, for a given change in dimensionality.

VI. MODEL CALCULATIONS

A. Exact diagonalization of an extended Hubbard model

In the previous section we obtained the network of interactions relevant for the Fabre CT salts by means of DFT calculations. We proceed now with model calculations in order to analyze the effect of correlations in these materials.

Since some of the phases realized in these materials are charge and spin ordered phases, we shall investigate charge and spin structure factors using a quarter (hole) filled extended Hubbard model,

$$H = -\sum_{\langle ij\rangle_8,\sigma} t_{ij}(c^\dagger_{i\sigma}c_{j\sigma} + c^\dagger_{j\sigma}c_{i\sigma}) + U\sum_i n_{i\uparrow}n_{i\downarrow} + \sum_{\langle ij\rangle_8} V_{ij}n_i n_j, \quad (6)$$

where the sum over $\langle ij\rangle_8$ is over the eight shortest distances between sites, t_{ij} [see Eq. (3)] are the corresponding hopping integrals, $c^\dagger_{i\sigma}$ ($c_{i\sigma}$) is the creation (annihilation) operator of a hole on the ith site with spin σ, and $n_i = n_{i\uparrow} + n_{i\downarrow}$ with $n_{i\sigma} = c^\dagger_{i\sigma}c_{i\sigma}$. U and V_{ij} are the on-site and the intersite Coulomb interactions.

In this section, we present numerical results for the Hamiltonian (6), using the electron hopping parameters (t_α with $\alpha = 0,\ldots,7$) as defined in Eq. (3) and obtained in Sec. V. We choose the on-site Coulomb interaction to be typical for this class of materials $U = 4t_0 \approx 1$ eV (U is of the order of the bandwidth $W \sim 1$ eV).[38] Since the arrangement of the molecules changes only slightly with pressure and temperature, we assume that the primary changes to the intersite interaction are based on the distance between the sites. This allows us to reduce the number of free parameters in our model; we scale V_α as a function of the distance r_α, $V_\alpha = V_0\frac{r_0}{r_\alpha}$, where the index α corresponds to the label of the hopping parameter between that pair of sites. The intersite interactions V_7 and V_3 are set to zero since we expect these terms to be strongly screened by the intermediate sites. Thus we only have two "free" parameters remaining, U and V_0. The Coulomb interaction along the chain V_0 has been estimated in a previous work as between $0.2\,U$ and $0.6\,U$.[38] Here we consider two cases, $V_0 = 0.5t_0$ (weak inter-site Coulomb repulsion) and $V_0 = 2t_0$ (strong intersite Coulomb repulsion), both using $U = 4t_0$. With this set of parameters, the ground state for a system of size $N = 16$ (4×4) sites with periodic boundary conditions (see Fig. 13) is found using exact diagonalization, as implemented in ALPS.[39,40] While similar methods have been applied to some members of this family of materials before, we note that calculating our parameters from Wannier orbitals allows us to have a more complete, realistic description of the interchain coupling.[33,41]

We compute dimer structure factors for charge and spin,

$$C_D(\mathbf{q}) = \frac{1}{N_d}\sum_{I,J}\langle n_I n_J\rangle e^{i\mathbf{q}\cdot(\mathbf{r}_J-\mathbf{r}_I)} \quad (7)$$

$$\text{with} \quad n_I = (n_i - n_{i+1})/2,$$

$$M_D(\mathbf{q}) = \frac{1}{N_d}\sum_{I,J}\langle m_I m_J\rangle e^{i\mathbf{q}\cdot(\mathbf{r}_J-\mathbf{r}_I)} \quad (8)$$

$$\text{with} \quad m_I = (m_i + m_{i+1})/2,$$

where I,J are the dimer indices with $i = 2(I-1)$ [and i and $i+1$ are the site (monomer) indices, see Fig. 13], N_d is the total number of dimers, $\mathbf{r}_I$ denotes the position of the Ith dimer, n_I is the charge difference between the sites in the dimer, and m_I is the total magnetization of dimers with $m_i = n_{i\uparrow} - n_{i\downarrow}$ the local magnetization.[33,41] Note that C_D quantifies the correlation between the charge polarization of dimers, while M_D measures the correlation between spins on dimers.

For the U and V values considered here, $C_D(\mathbf{q})$ has a maximum at $\mathbf{q} = (0,0)$ that corresponds to a charge order as shown in Fig. 13 (b). $M_D(\mathbf{q})$ has a maximum at $\mathbf{q} = (\pi,\pi)$ corresponding to a dimer antiferromagnetic order in both the in-chain and interchain directions [shown schematically in Fig. 13(b)].[33,41]

Here, we investigate charge and spin structure factors for various Fabre CT salt structures at different temperatures and pressures. To minimize the effects of experimental variability, we focus our analysis on the sets of structures synthesized and measured following the same procedure; the series of $(TMTTF)_2PF_6$ under pressure, and $(TMTTF)_2SbF_6$ for various temperatures. It is important to note that these results are for the zero-temperature ground state of a model Hamiltonian parameterised with the results from high-temperature crystal structure.

Both (0,0) charge order and (π,π) spin order are slightly suppressed with decreasing temperature and increasing pressure (see Figs. 14 and 15). This is in contrast to a previous work on a simpler model, which showed different trends for the charge and magnetic orders.[41] Charge order is strongly activated by increasing the strength of the intersite Coulomb interaction, V_0. The antiferromagnetic correlation is relatively weakly enhanced by increasing V_0. The changes in the correlation functions shown in Figs. 14 and 15 seem to be strongly connected to the degree of electronic dimerization $\partial_{\text{electronic}}$, which we show in Fig. 16. Lowering the temperature down to $T = 100$ K in $(TMTTF)_2SbF_6$ continuously decreases the electronic dimerization in these structures and thus suppresses intradimer charge order as well as interdimer antiferromagnetic order by making the one-dimensional chains more isotropic. The same observation holds for the increase of pressure on $(TMTTF)_2PF_6$ structures.

The charge and magnetically ordered states found for the Fabre CT salts with this model are consistent with the phase diagram for these materials, but we find no evidence of a phase transition as a function of pressure or intersite V's in this model. Note that this model cannot capture a

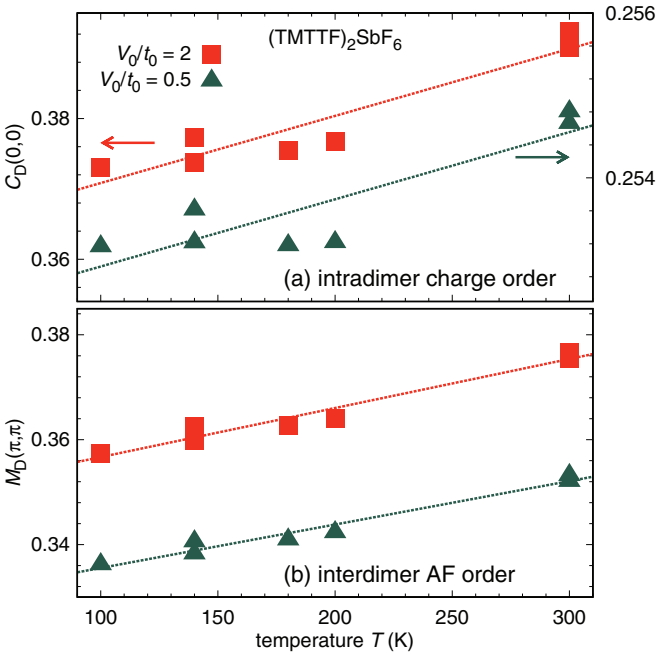

FIG. 14. (Color online) Structure factors as a function of temperature for $(TMTTF)_2SbF_6$. As the temperature is decreased the dimer charge and magnetic orders are somewhat suppressed. Simultaneously, the bandwidth and dimensionality increase. Thus decreasing temperature has the same effects as increasing pressure (see Fig. 15); the charge order is strongly activated by V_0, and the magnetic order is only weakly enhanced. The squares correspond to results with $V_0 = 2t_0$ while the triangles correspond to $V_0 = 0.5t_0$. The two points at 140 and 300 K are the results based on the two crystal structures we have at those temperatures.

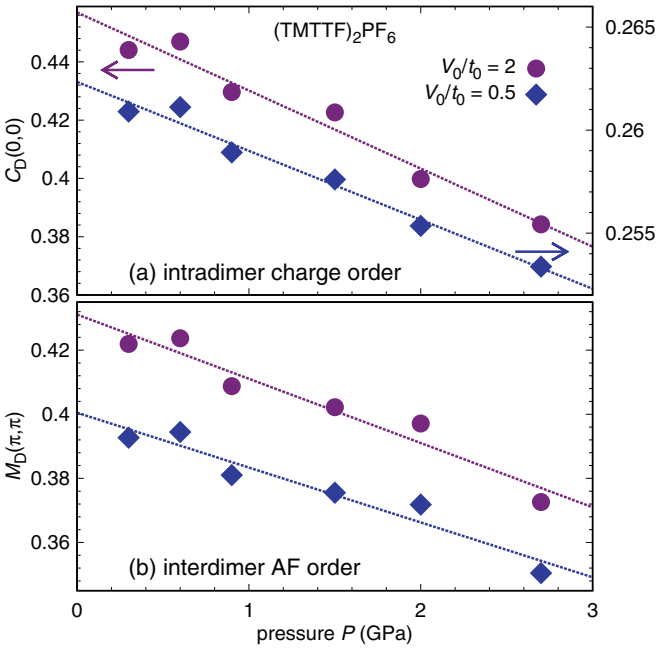

FIG. 15. (Color online) Structure factors as a function of pressure for $(TMTTF)_2PF_6$. As the pressure is increased the dimer charge and magnetic orders are somewhat suppressed. Simultaneously, the bandwidth and dimensionality increase [seen in Fig. 9(b)]. The charge order is strongly activated by the value of V_0, while the magnetic order is only weakly enhanced, and is even finite for $V_0 = 0$ (not shown). The circles correspond to results with $V_0 = 2t_0$, while the diamonds correspond to $V_0 = 0.5t_0$.

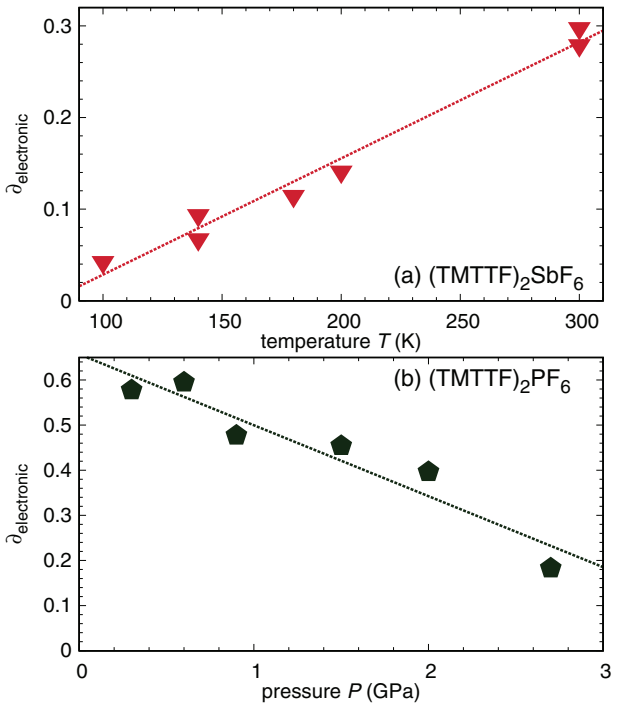

FIG. 16. (Color online) Electronic dimerization for (a) $(TMTTF)_2SbF_6$ as a function of temperature and (b) for $(TMTTF)_2PF_6$ under pressure.

spin-Peierls transition since no magnetoelastic coupling has been considered in the Hamiltonian.

In this analysis, we have concentrated on the $(0,0)$-charge and (π,π)-spin orders. However, in principle, there may be many kinds of charge order in these systems. For example, a maximum at $(0,\pi)$ would indicate a charge order that alternates in the b direction as well as in the a direction. Within the realistic parameter range explored here, we only observe the type illustrated in Fig. 13(b). We also note that to see some order on the level of the TMTTF monomers, we would need to compute a monomer structure factor.

VII. DISCUSSION

Summarizing our results, we observe that the dominant band structure parameters obtained in our work are generally consistent with those published for similar materials, however Ref. 42 finds quite different values for the electronic dimerization. Those authors compute the t values by constructing TMTTF HOMOs from an extended Hückel model (a tight-binding model for both the σ- and π-bonding systems of a molecule) and calculate the overlaps between them. This method does not allow for the charge reorganization and other effects in the crystal, which are better included by using the Wannier orbitals from DFT.

Table I shows that while structural dimerization tends to decrease with increasing pressure (both chemical and physical), the electronic dimerization only shows such a trend with physical pressure; there is no clear trend in electronic dimerization versus chemical pressure. Under chemical pressure, many aspects of the molecular arrangement can change (such as spacing and staggering), and there is no guarantee that they change smoothly with any one parameter of the anion, such as volume. This is clearest in the series of anions $(SbF_6)^-$, $(AsF_6)^-$, $(PF_6)^-$ at room temperature. As the anion size decreases (equivalent to increasing chemical pressure) the electronic dimerization shows no trend, while the structural dimerization decreases. It is important to note that the dimensionality (also computed from the electronic hopping parameters) shows a clear trend of increasing with increasing chemical and physical pressure; a trend that has been observed experimentally in $(TMTTF)_2PF_6$ and $(TMTTF)_2AsF_6$.[13,35] As the temperature of $(TMTTF)_2SbF_6$ is increased, it shows a clear increase in both structural and electronic dimerization.

Our model calculations show that while charge order is strongly activated by the inter-site Coulomb interaction V, the magnetic order is weakly enhanced. We also see a weak suppression of both kinds of order as the pressure is increased, and as the temperature is decreased.

To reproduce and understand the full phase diagram of these strongly correlated materials, one needs estimates of the Coulomb parameters. It is well known that molecular Coulomb parameters are overestimates for organic crystals; within the crystal, the interactions are strongly screened.[43–45] There are several promising approaches to calculating the screened Coulomb parameters, each with their own costs and benefits.[45,46] This will be addressed in a future work.

VIII. CONCLUSIONS

We have examined the structural and electronic properties of a set of Fabre charge transfer salts with crystal structures measured at different temperatures and pressures. By considering *ab initio* density functional theory calculations, we obtain a comparable set of physically meaningful electron hopping parameters. In these results, we identify some general trends: the structural dimerization is higher for the room-temperature systems, the electronic dimerization decreases with increasing pressure, the systems are more two-dimensional at lower temperatures and higher pressures, and this change in dimensionality is reflected in the degree of order in our model Hamiltonian. With this set of parameters, one can systematically investigate the differences between these materials in a model Hamiltonian.

It is possible that the variations seen in the electronic structure (such as the change in dimensionality) are responsible for tuning the ground states through the various phases accessible in these materials. However, ideally one would like a similarly systematic set of many-body interaction parameters as well as the one-body parameters given here.

ACKNOWLEDGMENTS

A.J., H.O.J., and R.V. thank the Deutsche Forschungsgemeinschaft for financial support through grant SFB/TR 49 and the Center for Scientific Computing (CSC, LOEWE-CSC) in Frankfurt for computing facilities.

[1]D. Jérome, Science **252**, 1509 (1991).
[2]H. Mori, J. Phys. Soc. Jpn. **75**, 051003 (2006).
[3]S. Yasuzuka and K. Murata, Sci. Technol. Adv. Mater. **10**, 024307 (2009).
[4]B. Köhler, E. Rose, M. Dumm, G. Untereiner, and M. Dressel, Phys. Rev. B **84**, 035124 (2011).
[5]T. Kawakami, T. Taniguchi, S. Nakano, Y. Kitagawa, and K. Yamaguchi, Polyhedron **22**, 2051 (2003).
[6]W. Yu, F. Zhang, F. Zamborszky, B. Alavi, A. Baur, C. A. Merlic, and S. E. Brown, Phys. Rev. B **70**, 121101 (2004).
[7]N. Doiron-Leyraud, P. Auban-Senzier, S. R. de Cotret, K. Bechgaard, D. Jérome, and L. Taillefer, Physica B **405**, S265 (2010).
[8]K. C. Kandpal, I. Opahle, Y.-Z. Zhang, H. O. Jeschke, and R. Valentí, Phys. Rev. Lett. **103**, 067004 (2009).
[9]H. O. Jeschke, M. de Souza, R. Valentí, R. S. Manna, M. Lang, and J. A. Schlueter, Phys. Rev. B **85**, 035125 (2012).
[10]Single crystals of $(TMTTF)_2PF_6$ and $(TMTTF)_2SbF_6$ were grown electrochemically in single or double H-type glass cells at room temperature. A constant voltage of 0.9–1.1 V was applied between platinum electrodes of approximately 5×10 and 15×20 mm^2, respectively, resulting in a starting current through the solution of about 14 μA. Needle-shaped single crystals of several millimeters in length and less than a millimeter in width are ready to harvest in about 1–4 weeks for $(TMTTF)_2SbF_6$ and 5–10 weeks for $(TMTTF)_2PF_6$. Structural investigations on $(TMTTF)_2X$ with $X = PF_6$ and SbF_6 under ambient conditions and down to 100 K were performed at Universität Stuttgart using a Kappa CCD Bruker AXS diffractometer. Diffraction angles θ of 0.41°–28.28° were considered while irradiating with a wavelength of $\lambda = 0.71073$ Å. The obtained R values vary from 0.036 to 0.062. The pressure dependent x-ray diffraction data for $(TMTTF)_2PF_6$ were collected at the ID09A beamline of the European Synchrotron Radiation Facility in Grenoble using a diamond anvil cell. A wavelength of 0.413 Å was irradiated with a diffraction angle θ of about 25°. X-ray diffraction patterns were collected on an imaging plate MAR345 detector by rotating the crystal from −30° to +30° with 2° steps, and analyzed using the XDR package.[11] The refinement of the atomic positions was performed by the SHELX software.[12,13] Gaseous helium was used as the pressure transmitting medium; the pressure in the cell was determined *in situ* by the ruby luminescence method.[14] Typical R values are in the range of 0.07–0.08.
[11]W. Kabsch, J. Appl. Cryst. **26**, 795 (1993).
[12]A. Pashkin, M. Dressel, S. G. Ebbinghaus, M. Hanfland, and C. A. Kuntscher, Synth. Met. **159**, 2097 (2009).
[13]E. Rose, C. Loose, J. Kortus, A. Pashkin, C. A. Kuntscher, S. G. Ebbinghaus, M. Hanfland, F. Lissner, T. Schleid, and M. Dressel, J. Phys.: Condens. Matter **25**, 014006 (2013).
[14]H. K. Mao, J. Xu, and P. M. Bell, J. Geophys. Res. **91**, 4673 (1986).
[15]K. Koepernik and H. Eschrig, Phys. Rev. B **59**, 1743 (1999).
[16]J. P. Perdew, K. Burke, and M. Ernzerhof, Phys. Rev. Lett. **77**, 3865 (1996).
[17]G. Kresse and J. Hafner, Phys. Rev. B **47**, 558 (1993).
[18]G. Kresse and J. Furthmüller, Comput. Mat. Sci. **6**, 15 (1996).
[19]P. E. Blöchl, Phys. Rev. B **50**, 17953 (1994).
[20]G. Kresse and D. Joubert, Phys. Rev. B **59**, 1758 (1999).
[21]S. Grimme, J. Comput. Chem. **27**, 1787 (2006).
[22]T. Granier, S. Gallois, L. Ducasse, A. Fritsch, and A. Filhol, Synth. Met. **24**, 343 (1988).
[23]B. Liautard, S. Peytavin, G. Brun, and M. Maurin, Cryst. Struct. Commun. **11**, 1841 (1982).
[24]J. L. Galigné, B. Liautard, S. Peytavin, G. Brun, J. M. Fabre, E. Torreilles, and L. Giral, Acta. Cryst. B **34**, 620 (1978).
[25]B. Liautard, S. Peytavin, G. Brun, D. Chasseau, J. M. Fabre, and L. Giral, Acta. Cryst. C **40**, 1023 (1984).
[26]J. L. Galigné, B. Liautard, S. Peytavin, G. Brun, M. Maurin, J. M. Fabre, E. Torreilles, and L. Giral, Acta. Cryst. B **35**, 1129 (1979).
[27]D. Pedron, R. Bozio, M. Meneghetti, and C. Pecile, Phys. Rev. B **49**, 10893 (1994).
[28]P. M. Grant, Phys. Rev. B **26**, 6888 (1982).
[29]M.-H. Whangbo, W. M. W., Jr., R. C. Haddon, and R. Wudl, Solid State Commun. **43**, 637 (1982).
[30]L. Ducasse, M. Abderrabba, J. Hoarau, M. Pesquer, B. Gallois, and J. Gaultier, J. Phys. C: Solid State Phys. **19**, 3805 (1986).
[31]J.-P. Pouget and S. Ravy, J. Phys. I France **6**, 1501 (1996).
[32]M. Dumm, A. Loidl, B. W. Fravel, K. P. Starkey, L. K. Montgomery, and M. Dressel, Phys. Rev. B **61**, 511 (2000).
[33]K. Yoshimi, H. Seo, S. Ishibashi, and S. E. Brown, Phys. Rev. Lett. **108**, 096402 (2012).
[34]M. de Souza, A. Brühl, J. Müller, P. Foury-Leylekian, A. Moradpour, J.-P. Pouget, and M. Lang, Physica B **404**, 494 (2009).
[35]A. Pashkin, M. Dressel, and C. A. Kuntscher, Phys. Rev. B **74**, 165118 (2006).
[36]A. Pashkin, M. Dressel, M. Hanfland, and C. A. Kuntscher, Phys. Rev. B **81**, 125109 (2010).
[37]F. Creuzet, T. Takahashi, and D. Jérome, J. Phys. Lett. **43**, 755 (1982).
[38]H. Seo, J. Merino, H. Yoshioka, and M. Ogata, J. Phys. Soc. Jpn. **75**, 051009 (2006).
[39]B. Bauer *et al.* (ALPS collaboration), J. Stat. Mech. (2011) P05001.
[40]A. F. Albuquerque *et al.* (ALPS collaboration), J. Mag. Mag. Mater. **310**, 1187 (2007).
[41]K. Yoshimi, H. Seo, S. Ishibashi, and S. E. Brown, Physica B **407**, 1783 (2012).
[42]Y. Nogami, T. Ito, K. Yamamoto, N. Irie, S. Horita, T. Kambe, N. Nagao, K. Oshima, N. Ikeda, and T. Nakamura, J. Phys. (Paris) IV **131**, 39 (2005).
[43]E. Scriven and B. J. Powell, J. Chem. Phys. **130**, 104508 (2009).
[44]E. Scriven and B. J. Powell, Phys. Rev. B **80**, 205107 (2009).
[45]L. Cano-Cortes, A. Dolfen, J. Merino, and E. Koch, Physica B **405**, S185 (2010).
[46]T. Miyake and F. Aryasetiawan, Phys. Rev. B **77**, 085122 (2008).
[47]See Supplemental Material at http://link.aps.org/supplemental/10.1103/PhysRevB.87.155139 for the full set of structural parameters for each of these materials and the full list of r_α corresponding to each t_α.